
# Palladium(II) and Platinum(II) Complexes of ((2-pyridyl)pyrazol-1-ylmethyl)benzoic Acids: Synthesis, Solid State Characterisation and Biological Cytotoxicity

Aidan P. McKay, Warrick K.C. Lo, Dan Preston, Gregory I. Giles, James D. Crowley, Jonathan E. Barnsley, Keith C. Gordon, David A. McMorran

PII: S0020-1693(16)30054-8
DOI: http://dx.doi.org/10.1016/j.ica.2016.02.038
Reference: ICA 16908

To appear in: *Inorganica Chimica Acta*

Received Date: 11 December 2015
Revised Date: 15 February 2016
Accepted Date: 18 February 2016

Please cite this article as: A.P. McKay, W.K.C. Lo, D. Preston, G.I. Giles, J.D. Crowley, J.E. Barnsley, K.C. Gordon, D.A. McMorran, Palladium(II) and Platinum(II) Complexes of ((2-pyridyl)pyrazol-1-ylmethyl)benzoic Acids: Synthesis, Solid State Characterisation and Biological Cytotoxicity, *Inorganica Chimica Acta* (2016), doi: http://dx.doi.org/10.1016/j.ica.2016.02.038

# Palladium(II) and Platinum(II) Complexes of ((2-pyridyl)pyrazol-1-ylmethyl)benzoic Acids: Synthesis, Solid State Characterisation and Biological Cytotoxicity.

Aidan P McKay[1], Warrick K C Lo[1], Dan Preston[1], Gregory I Giles[2], James D Crowley[1], Jonathan E Barnsley[1], Keith C Gordon[1] and David A McMorran[1]*

[1] Department of Chemistry, University of Otago, PO Box 56, Dunedin, New Zealand

[2] Department of Pharmacology and Toxicology, University of Otago, PO Box 56, Dunedin, New Zealand

davidm@chemistry.otago.ac.nz

**Abstract**

The new ligands 3-(3-(2-pyridyl)pyrazol-1-ylmethyl)benzoic acid **(L2)** and 5-(3-(2-pyridyl)pyrazol-1-ylmethyl)benzene 1,3-dicarboxylic acid **(L3)** are reported and the synthesis and characterisation of $[PdCl_2(\mathbf{L})]$ and $[PtCl_2(\mathbf{L})]$ complexes of these and the previously reported 4-(3-(2-pyridyl)pyrazol-1-ylmethyl)benzoic acid (**L1**) are described. In the solid state, the square planar complexes assemble *via* hydrogen bonding interactions involving COOH and M-Cl groups as well as by various π-stacking interactions involving the aromatic rings on the ligands and, notably, the chelate rings. Hirshfeld surface analysis has been used to gain insight into the assembly of the molecules. Preliminary studies of the biological cytotoxicity of the $[PtCl_2(\mathbf{L})]$ complexes against A549 and MDA-MB-231 cancer cell lines are reported.

## 1. Introduction

The development of an understanding of the myriad factors that drive how molecules assemble together into the solid state continues to be an important area of study in chemistry [1-6]. Key to such an understanding is a cataloging of the different possible interactions for a given set of molecular functionalities, or synthons, and a determination of the predictability of assembly motifs for such functionalities. Central to such a determination is the nature of the intermolecular force that drives the synthon-synthon interaction. Of the various intermolecular forces available, hydrogen

bonding has emerged as an important player, due to the strength and directionality of the interaction, and also the ease with which hydrogen bond donors and/or acceptors can be synthetically incorporated into molecules of interest [7]. The carboxylic acid (COOH) group, for example, has been shown to form $R^2_2(8)$ homodimers [8] in half of all structurally characterised compounds containing only carboxylic acid functionalities [9]. Interactions involving π systems have also received increasing attention [10]. While these tend to be weaker than hydrogen bonds, they also have a degree of directionality and, given the widespread use of aromatic rings in the frameworks of organic and inorganic molecules, π-stacking interactions play a significant role in the solid state assembly of many reported structures.

As the field of crystal engineering matures, systems that include more than one type of hydrogen bonding motif have begun to be explored, with the aim of determining a hierarchy of functionalities in terms of their hydrogen bond donor or acceptor abilities. For example, Vishweshwar *et al.* have shown that, in structural studies on pyridine and pyrazine monocarboxylic acids, the OH···N hydrogen bonding drives molecular assembly, rather than $R^2_2(8)$ dimer formation [11] and Du *et al.* have reported similar results in their studies on cocrystallisation of dipyridyl species with dicarboxylic acids [12]. Very recently, Duggirala *et al*. have shown that charge assisted hydrogen bonds between phenol groups and chloride anions prevail over COOH···Cl hydrogen bonds or $R^2_2(8)$ dimer formation in cocrystallisation experiments [13]. Such studies allow for the development of a quantitative ranking of, for example, hydrogen bond donors, where structural data from the Cambridge Structural Database (CSD) is used in combination with appropriate calculations [14].

We have recently reported the synthesis of 4-(3-(2-pyridyl)pyrazol-1-ylmethyl)benzoic acid (**L1**), which combines two nitrogen donors in a potential metal-chelating motif and a distal carboxylic acid group separated by a flexible methylene hinge [15]. The X-ray structure of **L1** showed that the molecules assembled *via* OH···N hydrogen bonds (between the COOH group of one molecule and the pyridine nitrogen of the next) into helical chains (consistent with the results of Vishweshwar *et al.* and Du *et al.*) – the helicity arising from the prochirality that the methylene hinge imparts to the ligand. Upon reaction of silver(I) salts with **L1**, $[Ag(\mathbf{L1})_2]^+$ complexes were obtained, in which the silver ion adopted a distorted tetrahedral geometry and the **L1** ligands wrapped around the metal such that chiral metallosynthons were generated. Hydrogen bonding interactions, either directly between the COOH groups of adjacent molecules or between COOH and solvent or counterion species, assemble these into either one-dimensional helical or *meso*-helical chains.

We were interested in extending these studies to square planar metal-based systems, and also in modifying the basic structure of the ligand. To this end, we herein report the new ligands 3-(3-(2-pyridyl)pyrazol-1-ylmethyl)benzoic acid **(L2)** and 5-(3-(2-pyridyl)pyrazol-1-ylmethyl)benzene 1,3-dicarboxylic acid **(L3)**, where the position, and number, of the COOH group(s) has been varied compared to **L1** (Scheme 1). Initially we attempted to prepare $[Pd(\mathbf{L})_2]^{2+}$ complexes, expecting that the palladium(II) ions would prefer a square planar geometry. However, these attempts were unsuccessful, due, we believe, to the steric clash between the methylene groups on the two ligands (in a *trans* arrangement) or the methylene group and a pyridine CH group (in a *cis* arrangement). This result is consistent with the literature: while a small number of palladium(II) and/or platinum(II) complexes containing pyridylpyrazole-type ligands have been reported [16-21], the only reports of $[M(\mathbf{L})_2]^{2+}$ systems are those where the N2 nitrogen of the pyrazole is unsubstituted [22-29]. We therefore moved our focus to square planar complexes of the type $[PdCl_2(\mathbf{L})]$ and $[PtCl_2(\mathbf{L})]$. These should not suffer the same steric issues as the $[M(\mathbf{L})_2]^{2+}$ complexes and also, being neutral rather than cationic, should modify the ways in which molecules will interact with each other in the solid state compared with the silver(I) complexes, where the role of the counterion was important. While intermolecular hydrogen bonding between COOH groups might be expected, as has been observed in related palladium systems [30-32], the potential M-Cl hydrogen bond acceptor might also be expected to play a role [5, 7, 33].

Synthesis and characterisation of the six $[MCl_2(\mathbf{L})]$ (M = Pd(II), Pt(II)) complexes is reported. The X-ray crystal structures of four of these, along with that of **L2**, were obtained and show a variety of packing arrangements, facilitated by a variety of intermolecular hydrogen bonding interactions (OH···N, OH···Cl, OH···O) as well as by π-π stacking interactions involving the chelate rings, a recently recognised [34-40] but probably not uncommon type of supramolecular motif. Indeed, it has been shown that, in certain cases, such interactions can be as strong as hydrogen bonds [38]. Hirshfeld surface analysis provides further insight into the nature of the intermolecular interactions in the complexes. Finally, given their similarity to the well-known chemotherapeutic agent cisplatin, the cytotoxicity of the complexes was explored.

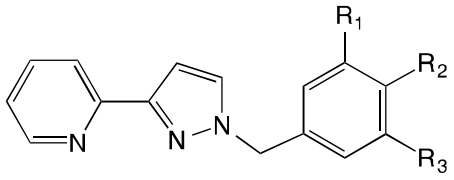


**L1**: $R_1$ = H, $R_2$ = COOH, $R_3$ = H
**L2**: $R_1$ = COOH, $R_2$ = H, $R_3$ = H
**L3**: $R_1$ = COOH, $R_2$ = H, $R_3$ = COOH

**Scheme 1**. The 2-pyridylpyrazole-based ligands discussed in this work.

## 2. Experimental

### *2.1. General methods*

The ligand 4-(3-(2-pyridyl)pyrazol-1-ylmethyl)benzoic acid (**L1**) [15] and the ligand precursors 3-bromomethylbenzoic acid [41], 1,3-dimethyl-5-(bromomethyl)benzene-1,3-dicarboxylate [42] and 2-(1*H*-pyrazol-3-yl)pyridine [43] were prepared by published procedures. *cis*-$[PdCl_2(CH_3CN)_2]$ was prepared by heating $PdCl_2$ in acetonitrile and *cis*-$[PtCl_2(dmso)_2]$ was prepared by adding dmso to an aqueous solution of $K_2PtCl_4$. All other chemicals were purchased commercially and used as received. $^1$H NMR and $^1$H-$^1$H COSY spectra were recorded on a 400 MHz Varian spectrometer at 298 K, referenced to the residual solvent signal. Microanalyses were performed at the Campbell Microanalytical Laboratory at the University of Otago. Mass spectra were collected on a Bruker micrOTOF-Q spectrometer. Infrared spectra were recorded on a Bruker ALPHA FT-IR spectrometer with an ALPHA P ATR measurement module.

### *2.2. Synthesis of 3-(3-(2-pyridyl)pyrazol-1-ylmethyl)benzoic acid (**L2**).*

2-(1*H*-Pyrazol-3-yl)pyridine (0.339 g, 2.33 mmol) and 3-bromomethylbenzoic acid (0.500 g, 2.33 mmol) were added to a solution of 40% aqueous NaOH (3.5 mL), benzene (10 mL), and $Bu_4NOH$ (4 drops), and the resulting solution was refluxed at 80 °C overnight. After cooling to room temperature, the colourless organic layer was separated from the yellow aqueous layer. The aqueous layer was then washed with ethyl acetate (2 × 10 mL) before being acidified to pH 3 using aqueous HCl (6 M), at which point a yellow precipitate formed. This precipitate was extracted into ethyl acetate (3 × 60 mL) that was then washed with water (2 × 50 mL) and brine (50 mL). The organic layer was then dried over magnesium sulfate before having the solvent removed under reduced pressure. Recrystallization from ethyl acetate/petroleum ether (40-60 $^o$C) gave **L2** as a pale brown

solid (0.224 g, 34%). Anal. calcd for $C_{16}H_{13}N_3O_2.0.25H_2O$ C, 67.71; H, 4.80; N, 14.80. Found: C, 67.94; H, 4.67; N, 14.72. $^1$H NMR (400 MHz, dmf-$d_7$): δ (ppm) = 5.61 (2H, s, $H_g$), 6.95 (1H, d, $J$ = 2.3 Hz, $H_e$), 7.30 (1H, ddd, $J$ = 7.4, 4.8, 1.2 Hz, $H_b$), 7.54 (1H, t, $J$ = 7.7 Hz, $H_h$), 7.64 (1H, dt, $J$ = 7.7, 1.5 Hz, $H_k$), 7.83 (1H, td, $J$ = 7.7, 1.8 Hz, $H_c$), 8.01 – 7.95 (3H, m, $H_d$, $H_j$ and $H_i$), 8.05 (1H, d, $J$ = 2.3 Hz, $H_f$), 8.60 (1H, dt, $J$ = 4.9, 1.3 Hz, $H_a$). HRESI-MS (dmf/MeOH): *m/z* calcd for $C_{16}H_{12}N_3O_2^-$: 278.0935 [**L2**-H]$^-$: found: 278.0930. Selected IR $\nu_{max}$ / cm$^{-1}$: 2415,1690, 1598, 1566, 1492, 1294, 768.

*2.3. 5-(3-(2-Pyridyl)pyrazol-1-ylmethyl)benzene 1,3-dicarboxylic acid (**L3**)*

2-(1*H*-pyrazol-3-yl)pyridine (0.500 g, 3.45 mmol) and 1,3-dimethyl-5-(bromomethyl)benzene-1,3-dicarboxylate (0.990 g, 3.45 mmol) were added to a solution of 40 % aqueous NaOH (5 mL), benzene (15 mL), and $Bu_4NOH$ (5 drops), and the resulting solution was refluxed at 80 °C overnight. After cooling to room temperature, the colourless organic layer was separated from the yellow aqueous layer. The aqueous layer was then washed with ethyl acetate (2 × 10 mL) before being acidified to pH 3 using aqueous HCl (6 M), at which point a white precipitate formed. The solvents were then removed *in vacuo* and the residue dissolved in *ca*. 1 mL of dmf. Addition of ethyl acetate gave a pale yellow solid, which was filtered off, washed with ethyl acetate and diethyl ether and dried (0.354 g, 32%). Anal. calcd for $C_{17}H_{13}N_3O_4.2H_2O$: C, 56.83; H, 4.77; N, 11.69. Found: C, 56.78; H, 3.82; N, 11.55. $^1$H NMR (400 MHz, dmf-$d_7$): δ (ppm) = 5.71 (2H, s, $H_g$), 6.96 (1H, d, $J$ = 2.3 Hz, $H_e$), 7.30 (1H, ddd, $J$ = 7.5, 4.9, 1.2 Hz, $H_b$), 7.83 (1H, td, $J$ = 7.7, 1.8 Hz, $H_c$), 7.97 (1H, dt, $J$ = 7.7, 1.8 Hz, $H_d$), 8.12 (1H, d, $J$ = 2.3 Hz, $H_f$), 8.21 (2H, m, $H_h$), 8.63-8.56 (2H, m, $H_a$, $H_i$). HRESI-MS (dmf/MeOH): *m/z* calcd for $C_{17}H_{12}N_3O_4^-$: 322.0833 [**L3**-H]$^-$; found: 322.0826 (100%). Selected IR $\nu_{max}$ / cm$^{-1}$: 2415, 1703, 1599, 1463, 1278, 766.

*2.4. Synthesis of [$PdCl_2$(**L1**)] (**1**)*

*cis*-[$PdCl_2(CH_3CN)_2$] (68 mg, 0.262 mmol) was added to a solution of **L1** (76 mg, 0.272 mmol) in methanol (25 mL). This solution was stirred and heated at 60 °C for 30 min during which time an orange precipitate formed in the yellow solution. The solution was then cooled to room temperature and the resulting precipitate was filtered, washed with methanol and diethyl ether, and dried *in vacuo* to give an orange solid, **1** (97 mg, 79%). Anal. calcd for $C_{16}H_{13}N_3O_2Cl_2Pd$: C, 42.09; H, 2.87; N, 9.20. Found: C, 41.54; H, 2.95; N, 9.13. $^1$H NMR (400 MHz, dmf-$d_7$) δ (ppm) = 6.41 (2H, s, $H_g$), 7.50 (1H, d, $J$ = 2.9 Hz, $H_e$), 7.58 (2H, d, $J$ = 8.1 Hz, $H_h$), 7.73 (1H, m, $H_b$), 8.04 (2H, d, $J$ = 8.0 Hz, $H_i$), 8.32 – 8.34 (2H, m, $H_c$, $H_d$), 8.44 (1H, d, $J$ = 2.9 Hz, $H_f$), 9.15 (1H, d, $J$ = 5.9, $H_a$). HRESI-MS

(*m/z*) (dmf/MeOH): calcd for $[PdCl_2(C_{16}H_{12}N_3O_2)]^-$: 455.9348, found: 455.9336. Selected IR $\nu_{max}$ / $cm^{-1}$: 2528, 1689, 1606, 1570, 1434, 1290, 766.

*2.5. Synthesis of [$PtCl_2$(**L1**)] (**2**)*

*cis*-$[PtCl_2(dmso)_2]$ (114 mg, 0.270 mmol) was added to a solution of **L1** (77 mg, 0.274 mmol) in methanol (20 mL). This solution was stirred and heated at 60 °C for 30 min during which time a pale yellow precipitate formed in the solution. After 30 min the reaction was cooled to 40 °C and was stirred overnight at this temperature. The solution was then cooled to room temperature and the resulting precipitate was filtered, washed with methanol and diethyl ether, and dried *in vacuo* to give a pale yellow solid, **2** (107 mg, 73%). Anal. calcd for $C_{16}H_{13}N_3O_2Cl_2Pt$: C, 35.24; H, 2.40; N, 7.71. Found: C, 34.94; H, 2.50; N, 7.45. $^1$H NMR (400 MHz, dmf-$d_7$) δ (ppm) = 6.52 (2H, s, $H_g$), 7.54 (1H, d, *J* = 3.0 Hz, $H_e$), 7.57 (2H, d, *J* = 8.1 Hz, $H_h$), 7.75 (1H, dt, *J* = 1.9, 7.6 Hz, $H_b$), 8.04 (2H, d, *J* = 8.0 Hz, $H_i$), 8.35 (1H, d, *J* = 7.8 Hz, $H_d$), 8.37 (1H, q, *J* = 7.9 Hz, $H_c$), 8.50 (1H, d, *J* = 3.0 Hz, $H_f$), 9.54 (1H, d, *J* = 6.0 Hz, $H_a$). HRESI-MS (*m/z*) (dmf/MeOH): calcd for $[PtCl_2(C_{16}H_{12}N_3O_2)]^-$: 543.9958, found: 543.9950. Selected IR $\nu_{max}$ / $cm^{-1}$: 2530, 1689, 1609, 1571, 1429, 1291, 766.

*2.6. Synthesis of [$PdCl_2$(**L2**)] (**3**)*

*cis*-$[PdCl_2(CH_3CN)_2]$ (38 mg, 0.145 mmol) was added to a solution of **L2** (40 mg, 0.143 mmol) in methanol (20 mL). This solution was stirred and heated at 60 °C for 30 min during which time an orange precipitate formed in the yellow solution. The solution was then cooled to room temperature and the resulting precipitate was filtered, washed with methanol and diethyl ether, and dried *in vacuo* to give a an orange solid, **3** (39 mg, 59%). Anal. calcd for $C_{16}H_{13}N_3O_2Cl_2Pd$: C, 42.09; H, 2.87; N, 9.20. Found: C, 41.90; H, 2.75; N, 9.14. $^1$H NMR (400 MHz, dmf-$d_7$) δ (ppm) = 6.41 (2H, s, $H_g$), 7.50 (1H, d, *J* = 2.9 Hz, $H_e$), 7.58 (1H, t, J = 7.7 Hz, $H_i$), 7.72 (1H, m, $H_b$), 7.79 (1H, d, *J* = 7.6 Hz, $H_h$, 8.00 (1H, d, *J* = 7.7 Hz, $H_j$), 8.10 (1H, s, $H_k$), 8.31 – 8.33 (2H, m, $H_c$,$H_d$), 8.48 (1H, d, *J* = 2.9 Hz, $H_f$), 9.15 (1H, d, *J* = 5.7 Hz, $H_a$). HRESI-MS (*m/z*) (dmf/MeOH): calcd for $[PdCl_2(C_{16}H_{12}N_3O_2)]^-$: 455.9348, found: 455.9340. Selected IR $\nu_{max}$ / $cm^{-1}$: 2530, 1714, 1605, 1440, 1291, 770.

*2.7. Synthesis of [$PtCl_2$(**L2**)] (**4**)*

*cis*-$[PtCl_2(dmso)_2]$ (62 mg, 0.147 mmol) was added to a solution of **L2** (40 mg, 0.145 mmol) in methanol (20 mL). This solution was stirred and heated at 60 °C for 30 min during which time a pale yellow precipitate formed in the solution. After 30 min the reaction was cooled to 40 °C and was stirred overnight at this temperature. The solution was then cooled to room temperature and the

resulting precipitate was filtered, washed with methanol and diethyl ether, and dried *in vacuo* to give a yellow crystalline solid, **4** (32 mg, 41%). Anal. calcd for $C_{16}H_{13}N_3O_2Cl_2Pt$: C, 35.24; H, 2.40; N, 7.71. Found: C, 35.45; H, 2.39; N, 7.61. $^1$H NMR (400 MHz, dmf-$d_7$) δ (ppm) = 6.52 (2H, s, $H_g$), 7.53 (1H, d, $J$ = 2.9 Hz, $H_e$), 7.57 (1H, t, $J$ = 7.7 Hz ,$H_i$), 7.75 (1H, ddd, $J$ = 7.6, 6.0, 1.9 Hz, $H_b$), 7.79 (1H, d, $J$ = 7.8 Hz, $H_h$), 7.99 (1H, d, $J$ = 7.8 Hz, $H_j$), 8.09 (1H, s, $H_k$), 8.41 – 8.31 (2H, m, $H_c$, $H_d$), 8.53 (1H, d, $J$ = 3.0 Hz, $H_f$), 9.53 (1H, d, $J$ = 5.9 Hz, $H_a$). HRESI-MS (*m/z*) (dmf/MeOH): calcd for $[PtCl_2(C_{16}H_{12}N_3O_2)]^-$: 543.9958, found: 543.9981. Selected IR $\nu_{max}$ / cm$^{-1}$: 2530, 1715, 1610, 1442, 1230, 766.

*2.8. Synthesis of [$PdCl_2$(**L3**)] (**5**)*

*cis*-$[PdCl_2(CH_3CN)_2]$ (40 mg, 0.155 mmol) was added to a solution of **L3** (50 mg, 0.155 mmol) in methanol (25 mL). This solution was stirred and heated at 60 °C for 30 min during which time an orange precipitate formed in the yellow solution. The solution was then cooled to room temperature and the resulting precipitate was filtered, washed with methanol and diethyl ether, and dried *in vacuo* to give an orange solid, **5** (59 mg, 76%). Anal. calcd for $C_{17}H_{13}N_3O_4Cl_2Pd.H_2O$ : C, 39.37; H, 2.92; N, 8.10. Found: C, 39.15; H, 2.84; N, 8.06. $^1$H NMR (400 MHz, dmf-$d_7$) δ (ppm) = 6.48 (2H, s, $H_g$), 7.53 (1H, d, $J$ = 2.8 Hz, $H_e$), 7.76-7.69 (1H, m, $H_b$), 8.30 (2H, d, $J$ = 1.6 Hz, $H_h$), 8.37 – 8.32 (2H, m, $H_c$, $H_d$), 8.56 (1H, d, $J$ = 2.9 Hz, $H_f$), 8.60 (1H, t, $J$ = 1.6 Hz, $H_i$), 9.15 (1H, dt, $J$ = 5.9, 1.1 Hz, $H_a$). HRESI-MS (dmf/MeOH): *m/z* calcd for $C_{17}H_{10}N_3O_4Pd^-$: 425.9719 [**5**-H]$^-$, found: 425.9730. Selected IR $\nu_{max}$ / cm$^{-1}$: 2530, 1710, 1605, 1440, 1275, 761.

*2.9. Synthesis of [$PtCl_2$(**L3**)] (**6**)*

*cis*-$[PtCl_2(dmso)_2]$ (65 mg, 0.155 mmol) was added to a solution of **L3** (50 mg, 0.155 mmol) in methanol (25 mL). This solution was stirred and heated at 60 °C for 30 min during which time a pale yellow precipitate formed in the solution. After 30 min the reaction was cooled to 40 °C and was stirred overnight at this temperature. The solution was then cooled to room temperature and the resulting precipitate was filtered, washed with methanol and diethyl ether, and dried *in vacuo* to give a bright orange solid, **6** (58 mg, 64%). Anal. calcd for $C_{17}H_{13}N_3O_4Cl_2Pt$: C, 34.65; H, 2.22; N, 7.13. Found: C,35.23; H, 2.20; N, 7.03. $^1$H NMR (400 MHz, dmf-$d_7$) δ (ppm) = 6.59 (2H, s, $H_g$), 7.57 (1H, d, $J$ = 3.0 Hz, $H_e$), 7.75 (1H, ddd, $J$ = 6.8, 5.9, 2.3 Hz, $H_b$), 8.29 (2H, d, $J$ = 1.6 Hz, $H_h$), 8.43 – 8.33 (2H, m, $H_c$, $H_d$), 8.66-8.56 (2H, m, $H_f$, $H_i$), 9.57-9.50 (1H, m, $H_a$). HRESI-MS (dmf/MeOH): *m/z* calcd for $C_{17}H_{12}N_3O_4PtCl_2^-$: 587.9843 [**6**-H]$^-$; found: 587.9872 (100%). Selected IR $\nu_{max}$ / cm$^{-1}$: 2530, 1687, 1627, 1448, 1257, 758.

*2.10. Cytotoxicity studies*

Reagents. 3-[4,5-Dimethylthiazol-2-yl]-2,5-diphenyltetrazolium bromide (MTT) and cell culture reagents were purchased from Life Technologies (Auckland, NZ). All other chemicals were obtained from Sigma-Aldrich (Auckland, NZ). Cell Culture: All cell lines were purchased from the American Type Culture Collection (ATCC, Manassas, VA, USA) and maintained in Dulbecco's Modified Eagles Medium (DMEM) enriched with 2% fetal bovine serum (FBS) and 1% antibiotic-antimycotic solution. All cells were cultured at 37 °C in a humidified atmosphere with 5% $CO_2$ levels. Cytotoxicity evaluation: Cell viability was assessed using the MTT assay.[44] Cell lines tested against were A549 (lung cancer) and MDA-MB 231 (breast cancer). Two 96 well plates were seeded with 5,000 cells per well, and the cells were left to adhere for 24 hours prior to treatment. The cells were then exposed to complexes solubilised in DMSO for 24 hours. To control for the effects of DMSO, all cell culture medium had a constant DMSO concentration of 0.5% (v/v). Following compound administration, cells were washed with phosphate buffer solution (PBS) and MTT (0.4 mg $mL^{-1}$ in DMEM) was added. After MTT incubation (3 hours), the medium was aspirated and the residual crystals were dissolved in DMSO. Cell number was then calculated at $\lambda$ = 550 nm. [45]

*2.11. X-ray crystallography*

X-ray data for **L2**, **3**.dmf, **4**, **5**.iPrOH and **6**.dmf were collected at 100 K on an Agilent Technologies Supernova system using Cu Kα radiation with exposures over 1.0°. X-ray data were treated using CrysAlisPro [46] software. X-ray crystal structures were solved using SIR-97 [47] and weighted full-matrix refinement on $F^2$ was carried out using SHELXL-97 [48] running within the WinGX [49] package. In each case all non-hydrogen atoms were refined anisotropically and hydrogen atoms were placed in calculated positions and refined using a riding model. Crystallographic and structure refinement data are provided in Table 1.

Colourless crystals of **L2** were grown by vapour diffusion of diisopropyl ether into an acetone solution. The structure was solved in the orthorhombic space group $Pna2_1$ and refined to an $R_1$ value of 3.9%. The asymmetric unit contains one molecule of **L2**. Yellow crystals of **3**.dmf were grown by vapour diffusion of diethyl ether into a dmf solution of **3**. The structure was solved in the monoclinic space group $P2_1/c$ and refined to an $R_1$ value of 4.2%. One molecule of **3** and one solvent dmf molecule are present in the asymmetric unit. Yellow crystals of **4** were obtained from the hot methanol reaction mixture. The structure was solved in the triclinic space group *P*-1 and refined to

an $R_1$ value of 2.3%. One molecule of **4** is present in the asymmetric unit. Yellow crystals of **5**.iPrOH were grown by layering isopropyl alcohol (*i*PrOH) onto a tetrahydrofuran solution of the complex. The structure was solved in the monoclinic space group $P2_1/c$ and refined to an $R_1$ value of 5.5%. One molecule of **5** and one solvent *i*PrOH molecule are present in the asymmetric unit. Pale yellow crystals of **6**.dmf were grown by vapour diffusion of diethyl ether into a dmf solution of **6**. The structure was solved in the triclinic space group *P*-1 and refined to an $R_1$ value of 8.7%. Two **6** molecules and two dmf solvent molecules are present in the asymmetric unit. The ellipsoids of atoms Cl3, C6, C13, C14, C15, C26, C28 and C31 became either elongated or flattened when refined anisotropically. These atoms were modelled with the ISOR command. The carboxylate groups containing C16, O1 and O2, C17, O3 and O4, and C34, O7 and O8 were disordered. A combination of ISOR and DFIX commands was used to model these carboxylate groups. The crystal lattice contained a small amount of diffuse electron density that could not be appropriately modelled. The SQUEEZE routine within PLATON was employed to resolve this problem, resulting in a void electron count of 84 that was assigned to two disordered diethyl ether solvent molecules (84 in total). CCDC numbers: 1441894 (**L2**), 1441895 (**3**.dmf), 1441896 (**4**), 1441897 (**5**.*i*PrOH) and 1441893 (**6**.dmf).

**Table 1**. Crystallographic data and structure refinement data

| | **L2** | **3**.dmf | **4** | **5**.iPrOH | **6**.dmf |
|---|---|---|---|---|---|
| chemical formula | $C_{16}H_{13}N_3O_2$ | $C_{19}H_{20}Cl_2N_4O_3Pd$ | $C_{16}H_{13}Cl_2N_3O_2Pt$ | $C_{20}H_{21}Cl_2N_3O_5Pd$ | $C_{20}H_{20}Cl_2N_4O_5Pt$ |
| formula weight | 279.29 | 529.69 | 545.28 | 560.70 | 662.39 |
| temperature (K) | 100.0(1) | 100.0(1) | 100.0(1) | 100.0(1) | 100.0(1) |
| wavelength (Å) | 1.54184 | 1.54184 | 1.54184 | 1.54184 | 1.54184 |
| crystal system | Orthorhombic | Monoclinic | Triclinic | Monoclinic | Triclinic |
| space group | *Pna*21 | $P2_1/c$ | *P*-1 | $P2_1/c$ | *P*-1 |
| *a* (Å) | 12.8393(9) | 10.0259(13) | 7.4273(3) | 17.8499(4) | 7.6293(2) |
| *b* (Å) | 21.6933(13) | 29.2584(3) | 9.9086(3) | 16.1431(4) | 17.9665(8) |
| *c* (Å) | 4.7745(4) | 7.0185(8) | 11.3726(4) | 7.7594(2) | 19.1008(9) |
| $\alpha$ (°) | 90 | 90 | 86.884(3) | 90 | 68.956(4) |
| $\beta$ (°) | 90 | 99.110(2) | 86.278(3) | 101.104(2) | 80.542(3) |
| $\gamma$ (°) | 90 | 90 | 78.323(3) | 90 | 84.648(3) |
| volume (Å$^3$) | 1329.83(17) | 2032.8(4) | 817.18(5) | 2194.03 | 2408.67(18) |
| Z | 4 | 4 | 2 | 4 | 4 |
| $D_{calcd}$ (Mg m$^{-3}$) | 1.395 | 1.731 | 2.216 | 1.697 | 1.827 |
| $\mu$ (mm$^{-1}$) | 0.774 | 10.036 | 19.201 | 9.395 | 13.269 |
| $T_{min}$, $T_{max}$ | 0.968, 0.995 | 0.529, 0.843 | 0.335, 0.520 | 0.692, 0.905 | 0.214, 0.699 |
| θ range (°) | 4.001-74.025 | 3.021-76.668 | 3.899-76.738 | 3.724-74.715 | 4.226-74.709 |
| reflections collected | 5695 | 15664 | 9827 | 23218 | 36493 |
| data/parameters | 2059/191 | 4237/265 | 3407/218 | 4461/284 | 9663/583 |
| $R_{int}$ | 0.0488 | 0.0543 | 0.0329 | 0.0704 | 0.0917 |
| $R_1$(w$R_2$) [$I > 2\sigma$] | 0.0390 (0.0913) | 0.0417 (0.1141) | 0.0228 (0.0575) | 0.0547 (0.1799) | 0.0866 (0.2342) |
| $R_1$(w$R_2$) (all data) | 0.0500 (0.0965) | 0.0437 (0.1195) | 0.0237 (0.0582) | 0.0653 (0.1864) | 0.1112 (0.2628) |

## 3. Results and discussion

The ligands **L1**-**L3** were prepared in moderate yields by a phase transfer alkylation reaction, as described previously [15, 51, 52] (Scheme 2). For **L2**, 3-bromomethyl benzoic acid, prepared in turn from 3-toluic acid [41], was refluxed with 2-pyridyl pyrazole in a mixture of benzene and 40% NaOH(aq), with a few drops of tetrabutylammonium hydroxide added to act as a phase transfer catalyst. To prepare **L3** 5-methylbenzene-1,3-dicarboxylic acid was converted to the dimethyl ester and then brominated following literature procedures [42]. The resulting 1,3-dimethyl-5-(bromomethyl)benzene-1,3-dicarboxylate was then submitted to the phase transfer alkylation reaction with 2-pyridyl pyrazole directly, as the highly basic reaction media not only enabled the coupling reaction, but also the de-esterification to the desired dicarboxylic acid **L3**.

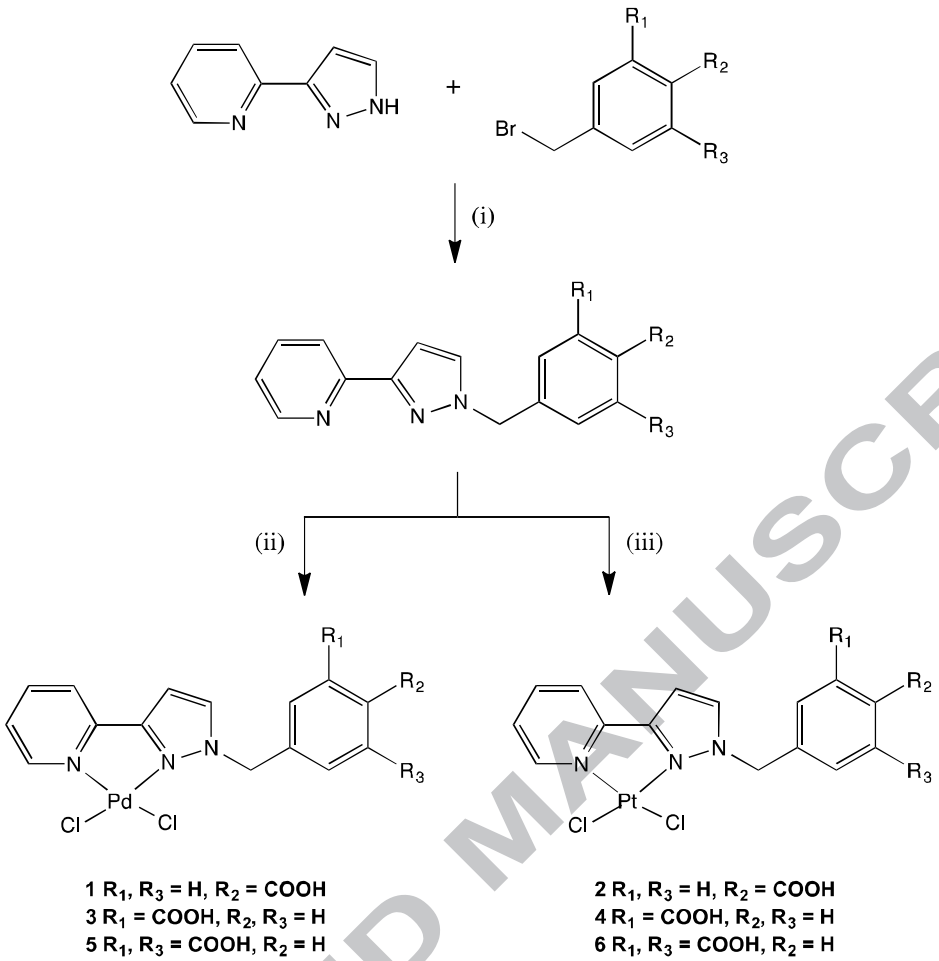


**Scheme 2**. Synthesis of ligands and complexes. (i) $C_6H_6$, 40% NaOH(aq), $Bu_4NOH$, reflux, overnight: (ii) $[PdCl_2(CH_3CN)_2]$, MeOH, 30 °C, 30 min: (iii) *cis*-$[PtCl_2(dmso)_2]$, MeOH, 60 °C, 30 min, 40°C, overnight.

The compositions of the ligands were confirmed by elemental analysis. High resolution electrospray ionisation (HRESI) mass spectra displayed peaks corresponding to $[\mathbf{L}\text{-H}]^-$ ions in each case (Figures S3 and S4). $^1$H NMR spectra were also consistent with the desired compounds and were similar to that of **L1** [15]. The complexes in turn were prepared in good yield by simply stirring the appropriate ligand with one equivalent of either $[PdCl_2(CH_3CN)_2]$ or $[PtCl_2(dmso)_2]$ in hot methanol (Scheme 2). The complexes are poorly soluble in most solvents, and dmf and dmso were found to be most useful for characterisation.

The $[MCl_2(\mathbf{L})]$ compositions of the complexes were confirmed by elemental analysis. HRESI mass spectra of dmf solutions of the palladium complexes **1**, **3** and **5** contained multiple peaks, including

ones corresponding to free ligand (Figures S5, S7, S9). Peaks corresponding to $[PdCl_2(\mathbf{L}\text{-H})]^-$ was observed for **1**, **3** and **5**, although for **5** this peak was very small. By contrast, the spectra of the Pt complexes comprised the $[PtCl_2(\mathbf{L}\text{-H})]^-$ peak almost exclusively (Figures S6, S8, S10). These results suggest that, in dmf solution under the conditions of the HRESI-MS experiment, the Pt(II) complexes are much more stable than the Pd(II) ones.

$^1$H NMR spectra of the complexes were recorded in dmf-$d_7$ solution. In each case significant coordination induced downfield shifts were observed for the signals for the protons on the pyridine and, to a lesser extent, the protons on the pyrazole rings (Figure 1 and S1, S2). While the signals due to the protons on the benzoic acid rings show almost no shift at all, consistent with the COOH group not being involved in the metal ion coordination, a large downfield shift is observed for the methylene protons ($H_g$). This is mostly likely due to their proximity to the chloride ions in the square planar complex. The fact that the signal for the methylene protons appears as a singlet also shows that, despite the prochiral nature of the ligand, in solution there is free rotation about the methylene group.

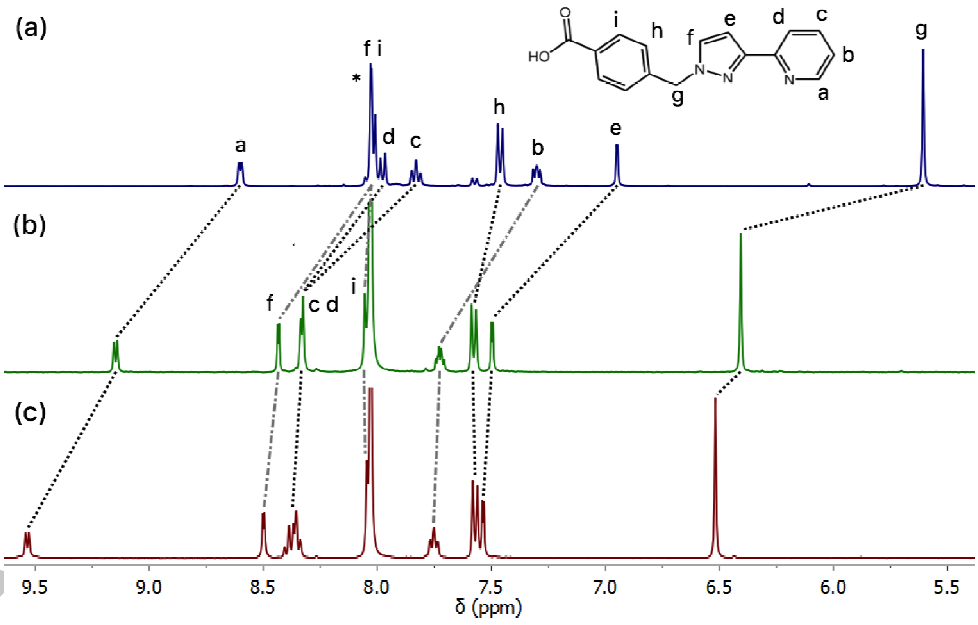


**Figure 1**. Stacked $^1$H NMR plot of **L1** (a), **1** (b) and **2** (c) in dmf-$d_7$ solution. * = dmf.

*3.1. Structural determinations*

To explore both how the methylene hinge influences the nature of the complexes, and how the various supramolecular synthons act to assemble the molecules into the solid, X-ray crystallography

was employed. While the solution studies show that there is free rotation about the methylene hinge in the complexes, in the solid state this will not be the case and chiral complexes should be formed. The relative orientations of the two ring systems in the ligands can be defined by two torsion angles $T_1$ and $T_2$, as described in Scheme 3. For any value of $T_1 \neq 0^o$ *endo* and *exo* faces of the pyridylpyrazole ring system can be defined, where the *endo* face is the one towards which the benzoic acid ring is oriented.

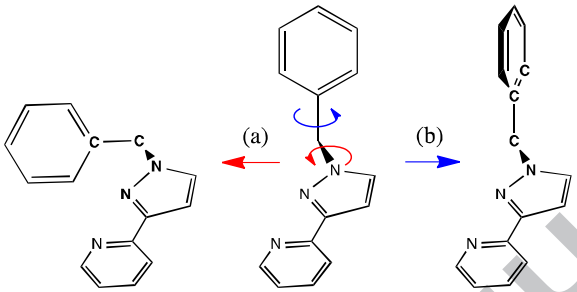


**Scheme 3.** Conformational flexibility in the ligands. (a) $T_1$ is defined by the torsion N2-N3-C9-C10, (b) $T_2$ is defined by the torsion N3-C9-C10-C11.

While **L3** could not be obtained in a suitable crystalline form, **L2** crystallises in the orthorhombic space group *Pna*$2_1$, with the asymmetric unit containing one molecule of **L2** (Figure 2). The pyridine and pyrazole rings, which are almost coplanar (the angle between the pyridine ring and pyrazole ring is 2.2$^o$), adopt the expected transoid disposition, thereby minimising repulsive interactions between the nitrogen lone pairs. The torsion angles $T_1$ and $T_2$ are 92.7$^o$ and -0.1$^o$, respectively with the COOH group oriented towards the pyridylpyrazole ring system.

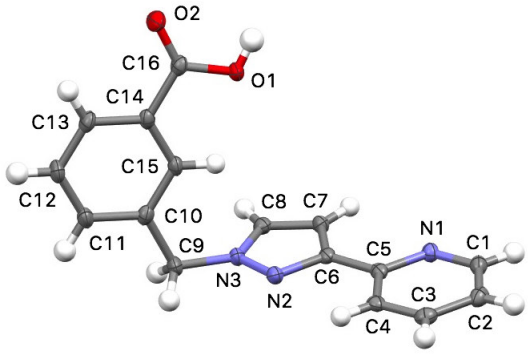


**Figure 2**. X-ray structure of **L2**. Ellipsoids are drawn at the 50% probability level.

Consideration of the extended structure shows that OH···$N_{py}$ hydrogen bonding interactions join adjacent molecules of **L2**. The O···N distance is 2.65 Å, the O-H···N angle is 171.3° (Table 3) and the angle between the pyridine and benzoic acid rings is 25.1°. Thus, rather than forming carboxylate dimers, molecules of **L2** assemble enantiospecifically into one-dimensional helical chains, which propagate along the crystallographic *c* axis with a pitch of 4.77 Å (corresponding to two molecules) (Figure 3). The chains are stabilised an offset π(py)···π(pz) stacking interaction (centroid···centroid distance is 3.606 Å, centroid displacement angle [53] is 37.7°) between one molecule and a second one two further along the chain. Similar chains of opposite helicity run parallel and interact with each other through two weak CH···O hydrogen bonds between methylene and aromatic hydrogens and carboxylic acid C=O groups (O···C = 3.156, 3.390 Å, O···H-C = 121.53, 140.63°, respectively).

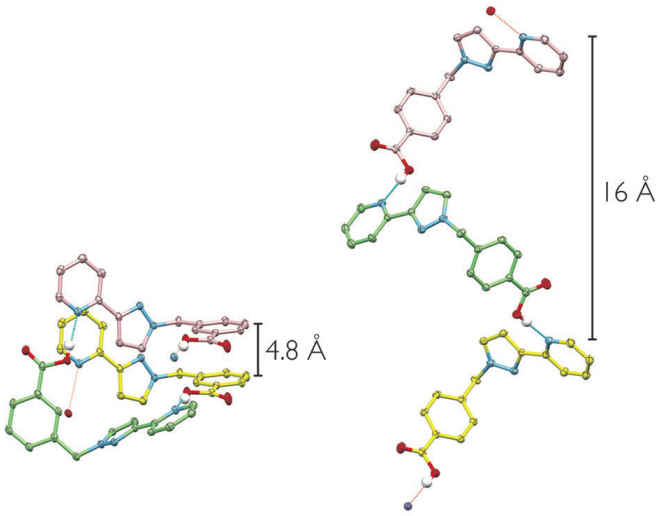


**Figure 3**. Extended structures of **L2** (left) and **L1** (right), showing helical chains. Hydrogen atoms not involved in hydrogen bonding are omitted for clarity.

The observed structure of **L2** is similar to that found for **L1** [15] in that they both adopt 1-dimensional helical chains in the solid state, with adjacent molecules assembling *via* O-H···N hydrogen bonds. However, the more distant placement of the COOH group in **L1** leads to a much less compact helix, with the pitch being 16.0 Å.

Frustratingly, despite numerous attempts, crystals suitable for X-ray analysis of **1** and **2** could not be obtained. However, suitable crystals of the remaining four complexes could be obtained. **3**

crystallises in the monoclinic space group $P2_1/c$ with the asymmetric unit containing one molecule of **3** and one dmf solvent molecule (Figure 4). Selected bond lengths and angles are listed in Table 2 and are unremarkable. The Pd(II) cation is coordinated by the N donors of the pyridine and pyrazole rings along with the two chloride ions and adopts a square planar geometry with a $\tau_4$ value of 0.06. ($\tau_4$ = 1 for a perfect tetrahedral geometry and 0 for a perfect square planar geometry [54]). The torsion angles $T_1$ and $T_2$ are 175.0° and 114.7°, respectively.

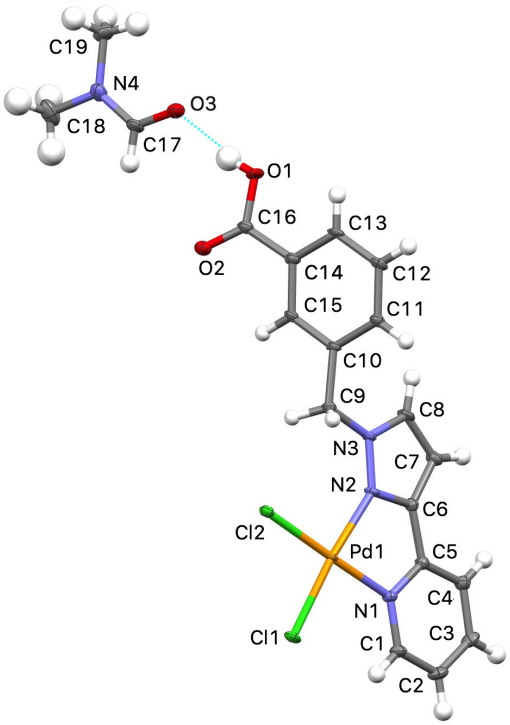


**Figure 4.** X-ray structure of **3**.dmf. Ellipsoids are drawn at the 50% probability level.

The solvent dmf molecule is hydrogen bonded to the COOH group of the ligand (O1···O3 2.577 Å, O1-H1A···O3 164.8°). The angle between the planes of the benzoic acid ring and the dmf molecule is 4.07°. However, this is the only strong hydrogen bonding interaction observed in the structure – rather the molecules assemble primarily due to π-stacking interactions. The pyridylpyrazole ring systems of molecules of alternating chirality stack along the crystallographic *c* axis in an *exo-endo* fashion, with the angle between adjacent ring system planes being 7.39° (Figure 5). The centroid···centroid distance between the pyridine rings is 3.739 Å (with a centroid displacement angle of 19.9°), values typical of a relatively strong π(py)···π(py) interaction [53]. However, the

distance between the centroids of the two chelate rings is smaller at 3.532 Å (with a centroid displacement angle is 4.3°), suggesting that, in concert with the π(py)···π(py) interaction, there is also a strong π(chelate)···π(chelate) interaction. Such interactions have recently been shown to be quite widespread in square-planar metal complexes and CSD searches have shown that there are three common motifs, related to the relative orientations of the two chelate rings (Scheme 4). The parallel motif has the torsion angle (τ) joining the chelate ring centroids *via* the metal ions, being *ca*. 0°, antiparallel has τ = *ca*. 180° and the cross motif has τ = *ca*. 90° [38, 55]. In complexes of the type discussed here, the antiparallel motif is most common, while the parallel motif is least common. The value for τ for **3** is 80.9°, so it adopts a cross motif.

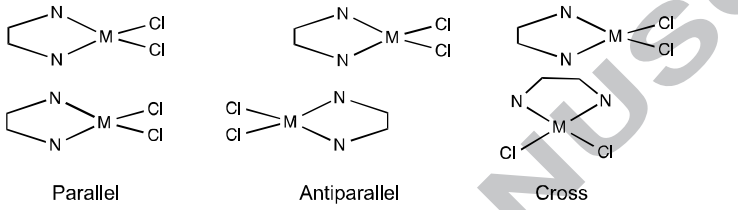


**Scheme 4**. Commonly observed structural motifs for π(chelate)···π(chelate) interactions.

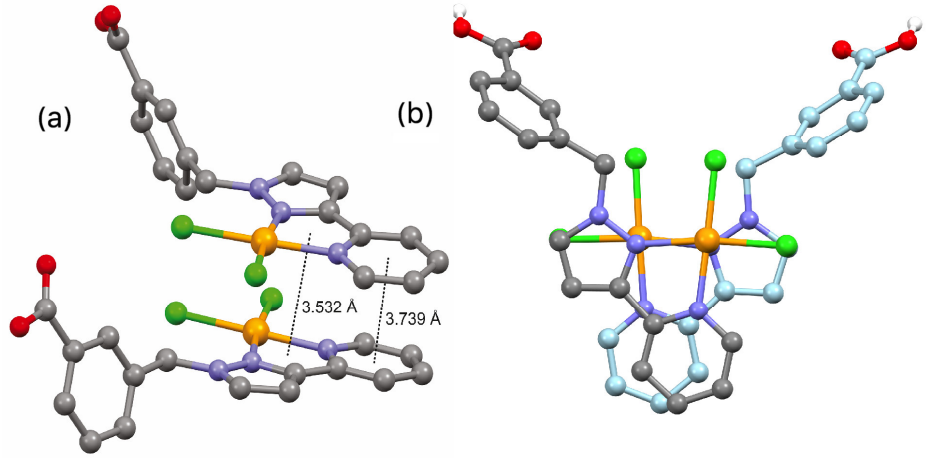


**Figure 5**. (a) View of the π-stacking of the pyridylpyrazole ring systems in **3**.dmf (dmf molecules omitted) and (b) view down the *c* axis, showing cross motif interactions between adjacent molecules.

These interactions are supplemented by two intermolecular CH···Cl hydrogen bonds: one to a CH on the benzoic acid ring (C···O = 3.656 Å, CH···O 147.35°) and one to a CH of the methylene bridge (C···O = 3.555 Å, CH···O 143.61°).

These stacks are directional, with each of the benzoic acid groups pointing in the same way (Figure 5b). This generates a V-shaped assembly, with the space between the 'arms' occupied by a second stack, held in place by a CH···Cl hydrogen bond between one of the chloride ligands and pyridyl ring CH (C···Cl = 3.495 Å, CH···Cl 123.27°) and a CH···O hydrogen bond between the C=O of a benzoic acid ring and a pyrazole ring CH (C···O = 3.428 Å, CH···O 158.96°) (Figure 6a). This nesting of stacks generates directional sheets along the crystallographic *a* axis. These sheets of nested stacks associate *via* pairs of $R^2_3(7)$ cyclic hydrogen bonding motifs, involving two CH hydrogens on one benzoic acid ring in one sheet and the benzoic acid-dmf OH···O hydrogen bond in the next, to generate the overall structure (Figure 6b).

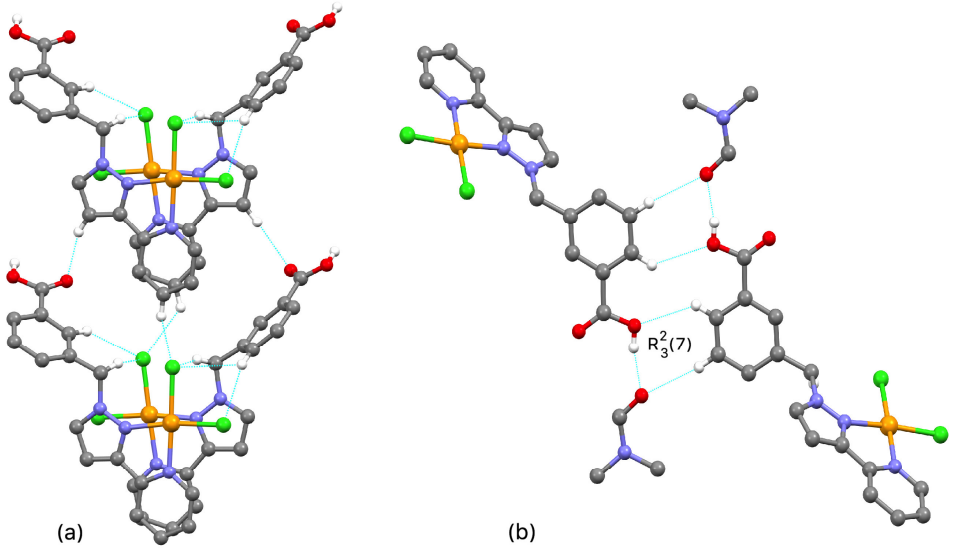


**Figure 6**. Hydrogen bonding interactions in **3**.dmf that connect the stacks of molecules into the three-dimensional structure. Hydrogen atoms not involved in hydrogen bonding are omitted for clarity.

**Table 2.** Selected bond lengths (Å), angles (°) and torsions (°)

| | **L2** | **3**.dmf | **4** | **5**.iPrOH | **6**.dmf [a] |
|---|---|---|---|---|---|
| M-Cl1 | | 2.2818(7) | 2.2908(8) | 2.2793(15) | 2.287(3), 2.273(6) |
| M-Cl2 | | 2.2843(8) | 2.2946(8) | 2.2781(14) | 2.295(3), 2.281(4) |
| M-N1 | | 2.047(3) | 2.040(3) | 2.047(5) | 2.033(10), 2.045(13) |
| M-N2 | | 2.049(3) | 2.047(3) | 2.069(5) | 2.056(10), 2.023(11) |
| Cl1-M-Cl2 | | 88.16(2) | 86.88(3) | 87.03(5) | 86.67(12), 87.3(2) |
| N1-M-N2 | | 79.51(10) | 79.45(11) | 79.8(2) | 79.2(4), 79.2(5) |
| Cl1-M-N2 | | 172.58(8) | 173.11(8) | 172.45(14) | 173.0(3), 172.3(4) |
| Cl2-M-N1 | | 178.54(7) | 176.32(8) | 179.37(14) | 178.0(3), 178.8(4) |
| $T_1$ (N2-N3-C9-C10) | 92.7 | 175.0 | 73.9 | 92.4 | -94.6, -76.8 |
| $T_2$ (N3-C9-C10-C11) | -0.1 | 114.7 | 45.6 | 73.3 | 3.2, -29.6 |

[a] Metrics for the two molecules in the asymmetric unit

**4** crystallises in the triclinic space group *P*-1 with the asymmetric unit containing a single molecule of **4** (Figure 7). The platinum(II) ion is coordinated by the N donors of the pyridine and pyrazole rings along with the two chloride ions (Table 2). The coordination sphere around the Pt is square planar, with a $\tau_4$ value of 0.06. The torsion angles $T_1$ and $T_2$ are 73.9° and 45.6°, respectively.

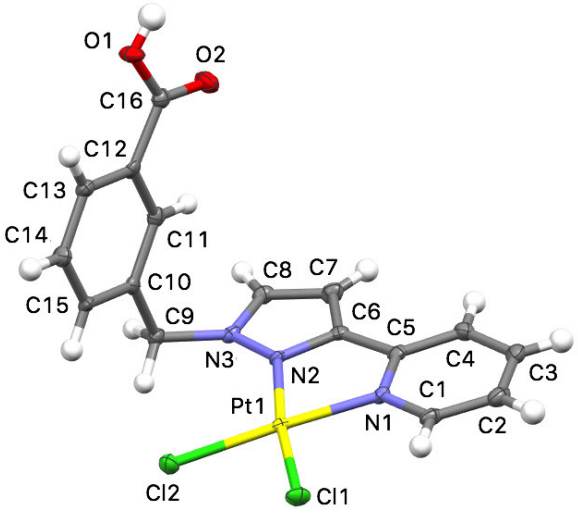


**Figure 7**. X-ray structure of **4**. Ellipsoids are drawn at the 50% probability level.

Molecules of **4** of alternating chirality assemble *via* a pair of *endo-endo* π(chelate)···π(py) interactions between the chelate ring of one molecule and the pyridyl ring of the next with the intercentroid distance being 3.828 Å and the ring-centroid displacement 22.47° (Figure 8). The motif could be described as offset antiparallel, with the τ value being 180° (by symmetry) – the proximity of the benzoic acid rings prevents a truly antiparallel arrangement. Additionally, each molecule also interacts with a second molecule of the same chirality *via* concerted *exo-exo* π(chelate)···π(chelate) (intercentroid distance 3.485 Å, ring centroid displacement 4.49°) and π(pz)···π(py) (intercentroid distance 3.669 Å, ring centroid displacement 20.60°) stacking interactions. These combine to generate stacks of molecules along the crystallographic *a* axis. The π-stacking interactions are complemented by a pair of CH···π interactions between CH protons on the pyridine ring on one molecule and the benzoic acid ring on the other (H···centroid 2.656 Å, CH···centroid 158.89°) (Figure 8a).

Adjacent stacks of molecules assemble *via* bifurcated $R^2_1(4)$ OH···Cl hydrogen bonds (O1···Cl1 3.24 Å, O1···Cl2 3.36 Å, O1-H1···Cl1 157.3°, O1-H1···Cl2 128.9°) and bifurcated $R^1_2(7)$ CH···O hydrogen bond between the C=O of the COOH group and hydrogens on the pyridine and pyrazole rings (C4···O2 3.25 Å, C7···O2 3.26 Å, C4-H4A···O2 169.1°, C7-H7A···O2 153.2°) in concert with $R^2_2(10)$ CH···O hydrogen bonds between the OH of the COOH group and a hydrogen on the benzoic acid ring (C13···O1 3.479 Å, C13-H13···O1 166.43°) (Figure 8b). Orthogonal π(acid)···π(acid) interactions (intercentroid distance 3.711 Å, ring centroid displacement 21.80°) generate the three-dimensional structure.

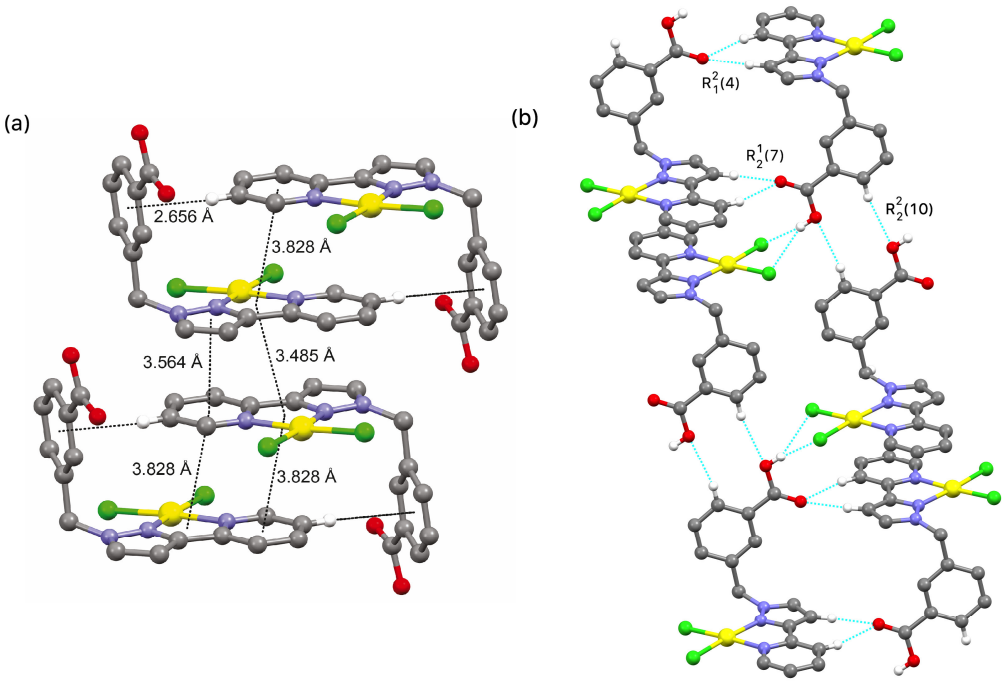


**Figure 8.** (a) π-stacking interactions and (b) hydrogen bonding interactions that assemble molecules of **4** in the solid state. Hydrogen atoms not involved in hydrogen bonding are omitted for clarity.

**5** crystallises in the monoclinic space group $P2_1/c$ with the asymmetric unit containing one molecule of **5** and one isopropanol solvent molecule (Figure 9). The palladium(II) ion is coordinated by the N donors of the pyridine and pyrazole rings along with the two chloride ions and adopts square planar geometry (Table 2), with a $\tau_4$ value of 0.08. The torsion angles $T_1$ and $T_2$ are 92.4° and 73.3°, respectively.

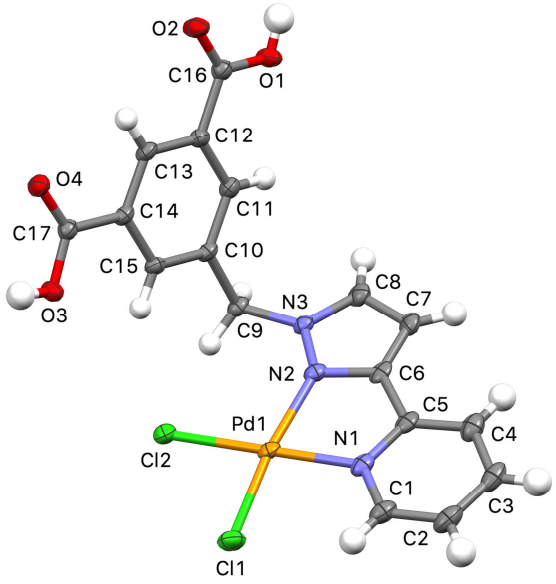


**Figure 9**. X-ray structure of **5**.*i*PrOH . Ellipsoids are drawn at the 50% probability level. Isopropanol solvent molecule omitted for clarity.

Molecules of **5** of the same chirality assemble *via* $R^2_2(8)$ hydrogen bond dimers, generating zig-zag chains along the crystallographic *b* axis (O1···O4 1.81 Å, O3···O2 1.78 Å, O1-H1A···O4 175.9°, O3-H3A···O2 170.4°) (Figure 10). The angle between adjacent benzoic acid rings is 8.6°. The chains are directional, with the $PdCl_2$ units all pointing the same way but lying on alternating sides of the plane generated by the benzoic acid rings. One of the chloride ions forms a hydrogen bond to the OH of the isopropanol solvate molecule (Cl1···O95 3.297 Å, Cl1···H95-O95 179.35°) and also a weaker hydrogen bond to a pyrazole CH on the neighbouring chain (Cl1···C7 3.550 Å, Cl1···H7-C7 140.77°). These Cl···CH hydrogen bonds assemble the zig-zag chains into sheets which lie parallel to the *ac* diagonal. The sheets in turn stack along the crystallographic *a* axis *via* two *exo-endo* π(chelate)···π(py) interactions (centroid···centroid distances are 3.438 and 3.442 Å, ring-centroid displacements are 4.13° and 4.12°) in an unusual offset pseudo-cross motif (τ = 121.5°).

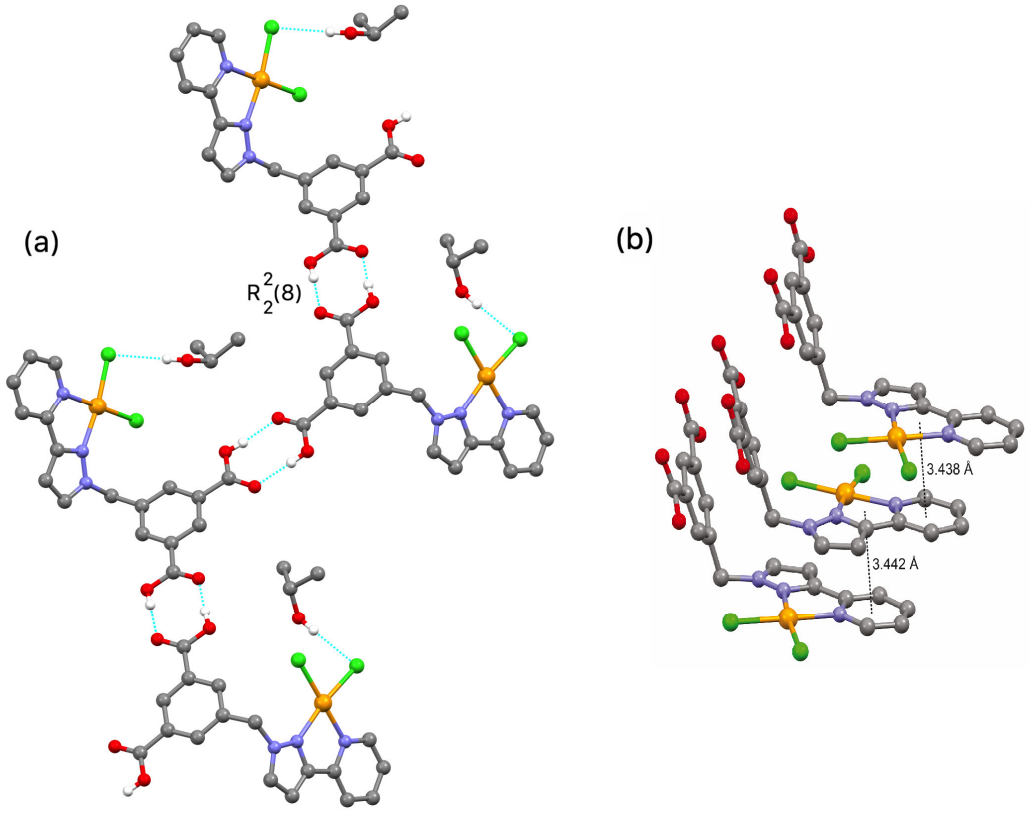


**Figure 10.** (a) Assembly of molecules of **5** into sheets *via* $R^2_2(8)$ hydrogen bond dimers, showing the OH···Cl hydrogen bonds to the isopropanol molecules; (b) Assembly of sheets *via* π(chelate)···π(py) stacking. Hydrogen atoms not involved in hydrogen bonding are omitted for clarity.

**6** crystallises in the triclinic space group *P*-1 with the asymmetric unit containing two molecules of **6**, each of which is hydrogen bonded to a dmf molecule *via* one of its COOH groups (Figure 11). The structures of the two molecules of **6** are similar. In each case, the platinum (II) ions are coordinated by the N donors of the pyridine and pyrazole rings and two chloride ions resulting in square planar geometries (Table 2) - the $\tau_4$ values for each of the complexes are 0.06. By contrast, the torsion angles $T_1$ and $T_2$ for the two molecules are quite different, with the values for the molecule containing Pt1 being -94.6° and 3.2°, respectively, whereas those for the molecule containing Pt2 are -76.8° and -29.6°, respectively.

Each molecule participates in two stacking interactions: an *exo-endo* π(chelate)···π(acid) interaction (intercentroid distance 3.453 Å, ring centroid displacement 0.90°) and an *endo-endo* π(py)···π(acid)

interaction (intercentroid distance 3.453 Å, ring centroid displacement 24.18°). These two π-stacking interactions generate stacks of molecules propagating along the crystallographic *a* axis (Figure 12).

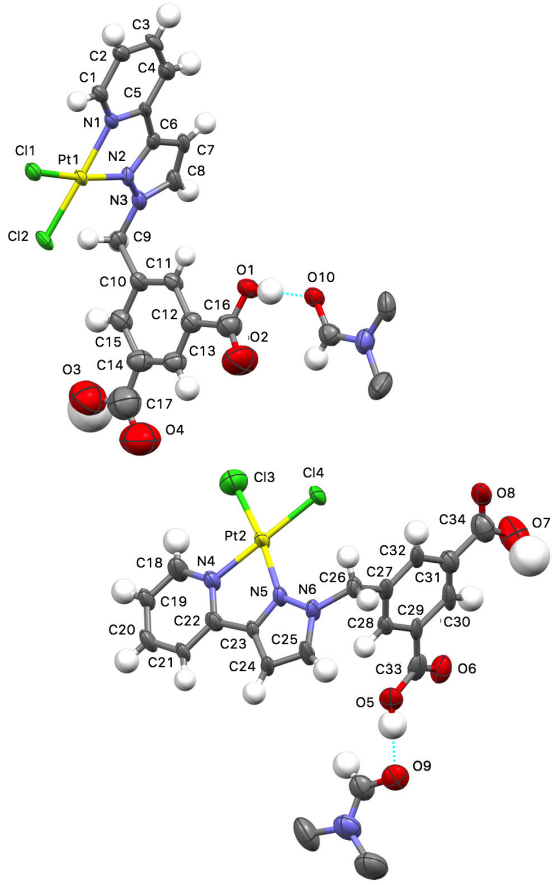


**Figure 11**. X-ray structure of **6**.dmf. Ellipsoids are drawn at the 50% probability level.

The molecule containing Pt1 further hydrogen bonds to a dmf *via* a *ca.* planar $R^2_2(7)$ motif with one strong hydrogen bond (O1···O10 2.561(15)Å, O1-H1A···O10 179.8°) and one weaker hydrogen bond (O2···C40 3.231(15) Å, O2···H40-C40 127.0°) with an angle between the COOH and NCHO planes of 15.6°. The second COOH group forms a weak O···HC hydrogen bond to the second dmf molecule (O4···C36 3.604 Å, O4···H36B-C36 156.32°). In contrast, the molecule containing Pt2 forms only a single hydrogen bond to the second dmf (O5···O9 2.58(2) Å, O5-H5A···O9 179.8°) as the angle between the COOH and NCHO planes is 86.4°.

The chloride ligands make a number of Cl···HC hydrogen bonding interactions. Cl1 hydrogen bonds to a methylene CH (Cl···C 3.761 Å, Cl···H-C 149.94°) and a pyrazole CH (Cl···C 3.571 Å, Cl···H-C

149.08°) within the stack and to a pyridine CH (Cl···C 3.675 Å, Cl···H-C 176.55°) in an adjacent stack. Cl2 hydrogen bonds to the CHO hydrogen of one of the dmf solvates (Cl···C 3.596 Å, Cl···H-C 172.64°) and to a pyridine CH (Cl···C 3.527 Å, Cl···H-C 129.31°) on an adjacent stack. Cl4 forms two hydrogen bonds, to a pyridine CH (Cl···C 3.683 Å, Cl···H-C 145.87°) within the same stack and to a pyridine CH (Cl···C 3.577 Å, Cl···H-C 158.07°) in an adjacent stack.

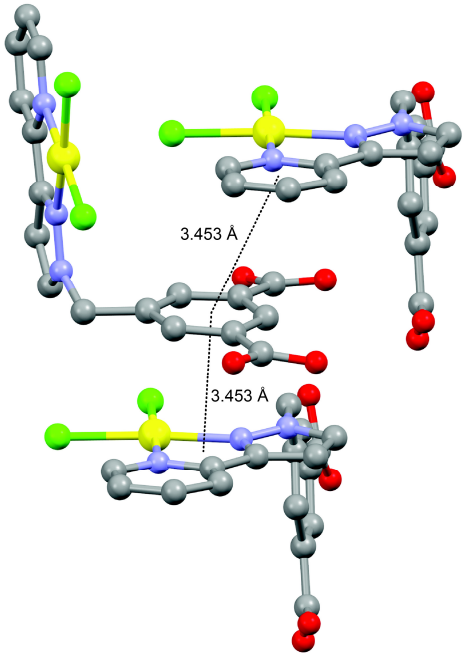


**Figure 12.** Stacking of molecules of **6** along the crystallographic *a* axis.

**Table 3**. Selected hydrogen bond data

| | D-H···A | d(H···A) / Å | d(D···A) / Å | ∠(DHA) / ° |
|---|---|---|---|---|
| **L2** | O1-H1A···N1#1 | 1.83 | 2.647(3) | 171.2 |
| **3**.dmf | O1-H1A···O3 | 1.78 | 2.577(3) | 164.8 |
| **4** | O1-H1A···Cl1#2 | 2.47 | 3.237(3) | 157.3 |
| | O1-H1A···Cl2#1 | 2.49 | 3.363(3) | 128.9 |
| **5**.*i*PrOH | O3-H3A···O2#3 | 1.78 | 2.589(6) | 170.4 |
| | O1-H1A-O4#4 | 1.81 | 2.626(6) | 175.9 |
| **6**.dmf | O1-H1A···O10 | 1.71 | 2.561(15) | 179.8 |
| | O5-H5A···O9 | 1.73 | 2.58(2) | 179.8 |

Symmetry transformations used to generate equivalent atoms: #1 –*x*+1, -*y*+2, *z*-1/2; #2 *x*-1, *y*+1, *z*; #3-*x*+1, *y*+1/2, -*z*+1/2; #4 –*x*+1, *y*-1/2, -*z*+1/2.

*3.2. Hirshfeld Surface Analysis*

Hirshfeld surfaces [57, 58] and their associated 2D-fingerprint plots were generated from the cif files for **L2** and complexes **3** – **6** using CrystalExplorer [59]. These provide a way to quantify the different types of intermolecular contacts between molecules in the crystal and so compare the importance of each type between the structures. Figure 13 shows the Hirshfeld surface and the 2D fingerprint plot for **L2.**

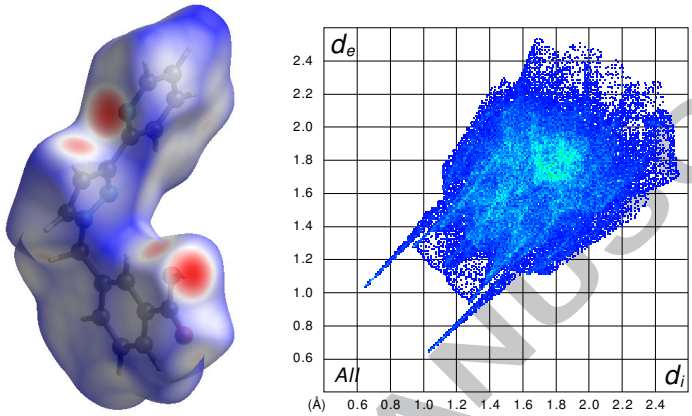


**Figure 13**. Hirshfeld Surface plot (superimposed over the X-ray structure) (left) and fingerprint plot (all interactions) (right) for **L2**.

The Hirshfeld surface displays short intermolecular contacts in red, contacts at about the van der Waals distance in white and regions with no close contacts in blue. Figure 13 shows large red patches at the pyridine nitrogen and the OH of the carboxylic acid, corresponding to the observed OH···N hydrogen bond. The smaller red regions correspond to a weaker interaction between the oxygen of the OH group and a CH hydrogen on the pyrazole ring of the neighbouring molecule. The fingerprint region plots $d_i$ *vs.* $d_e$, where these are the distances from the Hirshfeld surface to the nearest nuclei inside and outside the surface, respectively, with the colours changing from blue to green as the frequency with which a particular ($d_i$/$d_e$) increases. While the bulk of the contacts relate to general van der Waals contacts (H···H contacts account for 42.7% of all contacts), the $d_i$/$d_e$ values associated with the green region in the centre of the plot correspond to those expected for π-stacking interactions (7.7%), while the characteristic pair of spikes at the lower left correspond to the OH···N hydrogen bonding (12.7%).

Fingerprint plots for compounds **3** – **6**, summarising all the intermolecular interactions present in these structures, are shown in Figure 14 (and plots for each of the individual interaction types are presented in Figure S19-S23). In each case the characteristic features corresponding to certain types of interaction are highlighted, and the percentage of each type of interaction tabulated (Table S3). The plots are asymmetric for **3**, **5** and **6** due to presence of the solvent molecules in the structures, which were not included in the calculation of the Hirshfeld surface. In each case the interactions between molecules in the X-ray structures described above are found in the fingerprint plots, but the quantification of each type of interaction in the different structures allows for comparison between them. For example, while, in all cases, dispersive H···H are the predominant interactions (*ca.* 30% of all the interactions in each case), H···O and H···Cl hydrogen bonding interactions combined make up *ca.* 35% of total. Of these, the H···O percentage is greater, and the H···Cl percentage is smaller, for the palladium complexes **3** and **5**, than for the platinum complexes **4** and **6**. The fact that there is a greater percentage of H···O interactions in **4** and **6** might be expected, as these are the complexes with two COOH groups. The data further suggest that the Cl is a better hydrogen bond acceptor when coordinated to the palladium, which is consistent with the electron density calculations (Table S1), which show a larger electron density on the chlorines attached to palladium as compared to platinum. By contrast, the proportion of the total interactions attributable to π-stacking interactions (estimated by summing the contributions from the C···C, C···N, M···C and M···N interactions) range from 7.4% to 14.0%, significantly less than the hydrogen bonding. This perhaps surprising result may be due to the fact that, while the predominant motif for molecular assembly observed in the X-ray crystal structures is π-stacking (and, in particular, stacking involving the chelate rings), the interactions between these stacks is largely hydrogen bonding in nature and, across the crystal as a whole, these outweigh the π-stacking. The data in Figure 14 also reveal the significance of H···C interactions, with these accounting for between 12.0 and 15.3% of the interactions. These presumably arise from CH···π interactions between molecules (which appear as characteristic 'wings' on the plots). It is also interesting to note the diffuse nature of the plots for **5** and especially **6** in the top right hand corner, indicating less efficient packing of the molecules in the cases where **L3** is present. This presumably is a result of the utilisation of both COOH groups in the intermolecular hydrogen bonding: calculations using Mercury [60] confirm that the void volume (probe radius = 0.5 Å) in the structure of **6** (13.5%) is more than twice that of the other structures.

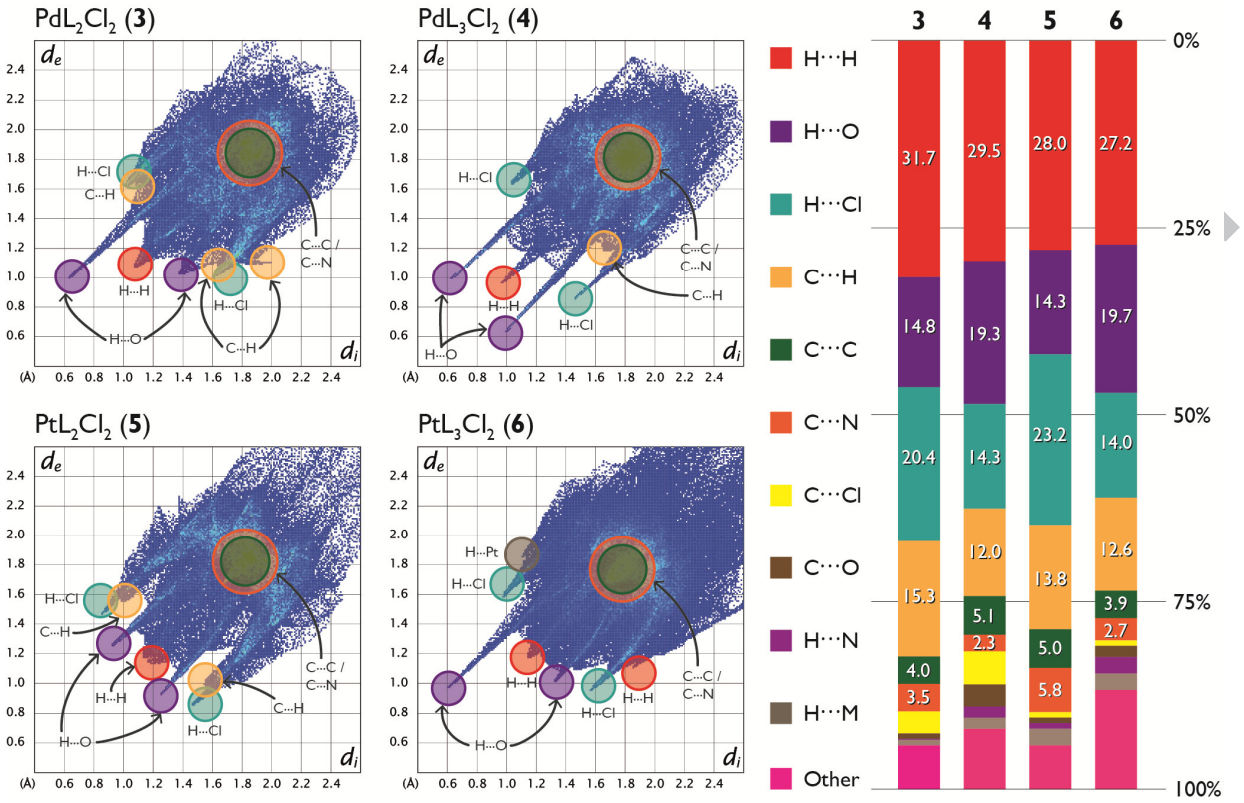


**Figure 14**. Fingerprint plots showing the important intermolecular interactions in the crystal packing of compounds **3 – 6**, with the associated percentages of each type of interaction.

*3.4. Biological Cytotoxicity*

Since the discovery of the therapeutic effects of cisplatin, there has been vigorous exploration of platinum(II) complexes as anticancer agents [61], with interest also in palladium(II) complexes.[62] While most attention has focussed on complexes with $N_2Cl_2$ donor sets, where the nitrogen donors are aliphatic or aromatic, and often part of a chelating ligand, systems with extra functionality to potentially enhance their effectiveness have also been explored [63-65]. Of particular relevance, Sun *et al.* have shown that Pd(II) and Pt(II) complexes of 2,2'-bipyridyl-5,5'-dicarboxylic acid and 2,2'-bipyridyl-4,4'-dicarboxylic acid possess appreciable cytotoxicity in both the neutral [66] and deprotonated [67] acid forms.

Preliminary studies indicated that the present palladium(II) complexes did not possess the requisite stability to act as cytotoxic agents (NMR spectra of dmso-$d_6$ solutions containing 5 equivalents histidine showed decomposition of the complexes). However, the platinum(II) complexes were

found to be more stable and were tested for cytotoxic effect against A549 (lung cancer) cells and cisplatin resistant [68] MDA-MB 231 (breast cancer) cells (against which cisplatin has an $IC_{50}$ = 9.4±0.3 μM [69] and 41.2±3.9 μM, [70] respectively). Unfortunately, the three platinum(II) complexes all exhibited low cytotoxicity against both cell lines ($IC_{50}$ > 60 μM) (Figure 15), suggesting that in their current form these compounds possess little potential as anticancer agents.

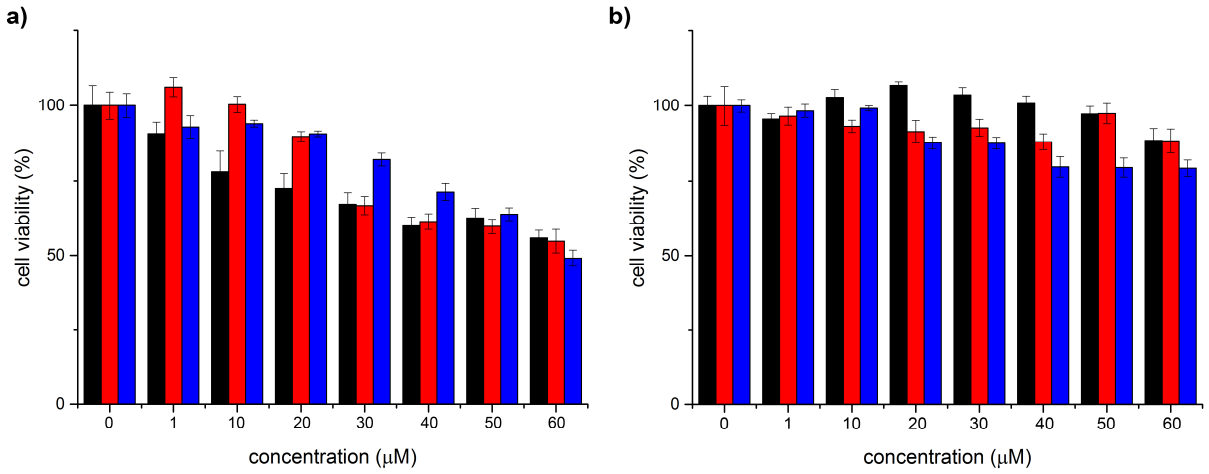


**Figure 15**. Cell viability ((a) A549, (b) MDA MB 231) plotted against varying concentrations of platinum(II) compounds. **2** (■), **4** (■), **6** (■). Cells were treated with 0 to 60 μM of compounds for 24 hours, and cell viability was assessed. Cell viability is expressed as mean ± standard error of mean, where n = 8.

## 4. Conclusions

Ligands **L1** – **L3** readily form square planar complexes of the type $[PdCl_2(\mathbf{L})]$ and $[PtCl_2(\mathbf{L})]$ that are usefully soluble only in dmf and dmso. X-ray crystallography shows that while the complexes adopt quite similar structures in the solid state (except for the rotation of the benzoic acid group with respect to the pyridylpyrazole ring system – Figure 15) the ways in which the molecules assemble within the crystal vary considerably. In general, molecules arrange into stacks, facilitated by π-stacking interactions involving (depending on the compound) all the available aromatic rings, as well as the chelate ring of the complex. The stacks are then assembled into the overall structure by means of hydrogen bonding interactions involving the COOH groups (donor and acceptor), the M-Cl acceptor as well as weaker hydrogen bonding involving CH donors. Hirshfeld surface analysis shows that these hydrogen bonding interactions account for about 35% of the total interactions within the structures.

Thus, while the initial aim of assembling the molecules primarily by means of the appended COOH groups and/or the chloride ligands was not realised (with the exception of **5**), this may be in part due to the inclusion of solvent molecules such as dmf (necessitated by the compounds' poor solubility), which competed for the hydrogen bond donors. It may also be the case that the π-stacking interactions, and in particular the π(chelate)-stacking interactions, in the current molecules are sufficiently strong to compete with the hydrogen bonding in these cases [38]. Studies to better understand the hierarchies of the intermolecular interactions in these systems are continuing.

**Acknowledgments**

DP and WKCL thank the University of Otago for PhD scholarships, Lisa Bucke is thanked for preparation of some of the figures and the University of Otago is acknowledged for financial support.

**Supporting Information**

$^{1}$H NMR spectra, mass spectra, details of the DFT calculations and Hirshfeld surfaces and fingerprint plots can be found in the Supporting Information.

**References**

[1] K. Biradha, R. Santra, Chem. Soc. Rev., 42 (2013) 950-967.
[2] G.R. Desiraju, J. Am. Chem. Soc., 135 (2013) 9952-9967.
[3] M.G. Goesten, F. Kapteijn, J. Gascon, CrystEngComm, 15 (2013) 9249-9257.
[4] M.W. Hosseini, in: Molecular tectonics. An approach to crystal engineering, CRC Press, 2012, pp. 231-254.
[5] P. Metrangolo, G. Resnati, Chem. Commun. (Cambridge, U. K.), 49 (2013) 1783-1785.
[6] A. Mukherjee, Cryst. Growth Des., 15 (2015) 3076-3085.
[7] Z.-T.W. Li, Li-Zhu, Hydrogen Bonded Supramolecular Structures, Springer, 2015.
[8] M.C. Etter, J.C. MacDonald, J. Bernstein, Acta Crystallogr B, 46 ( Pt 2) (1990) 256-262.
[9] O. Ivasenko, D.F. Perepichka, Chem. Soc. Rev., 40 (2011) 191-206.
[10] E.R.T. Tiekink, Zukerman-Schpector, J., The Importance of Pi-Interactions in Crystal Engineering, Wiley, 2012.
[11] P. Vishweshwar, A. Nangia, V.M. Lynch, J. Org. Chem., 67 (2002) 556-565.
[12] M. Du, Z.-H. Zhang, X.-J. Zhao, Cryst. Growth Des., 5 (2005) 1199-1208.
[13] N.K. Duggirala, G.P.F. Wood, A. Fischer, L. Wojtas, M.L. Perry, M.J. Zaworotko, Cryst. Growth Des., 15 (2015) 4341-4354.
[14] C.B. Aakeroey, K. Epa, S. Forbes, N. Schultheiss, J. Desper, Chem. - Eur. J., 19 (2013) 14998-15003.
[15] D.A. McMorran, Inorg. Chem., 47 (2008) 592-601.
[16] S.-Y. Chang, J. Kavitha, S.-W. Li, C.-S. Hsu, Y. Chi, Y.-S. Yeh, P.-T. Chou, G.-H. Lee, A.J. Carty, Y.-T. Tao, C.-H. Chien, Inorg. Chem., 45 (2006) 137-146.

[17] C.-S. Liu, X.-S. Shi, Acta Crystallogr., Sect. E: Struct. Rep. Online, 63 (2007) m2892, m2892/2891-m2892/2897.
[18] V. Montoya, J. Pons, V. Branchadell, J. Garcia-Anton, X. Solans, M. Font-Bardia, J. Ros, Organometallics, 27 (2008) 1084-1091.
[19] V. Montoya, J. Pons, J. Garcia-Anton, X. Solans, M. Font-Bardia, J. Ros, Inorg. Chim. Acta, 360 (2007) 625-637.
[20] V. Montoya, J. Pons, X. Solans, M. Font-Bardia, J. Ros, Inorg. Chim. Acta, 358 (2005) 2763-2769.
[21] M.-H. Sie, Y.-H. Hsieh, Y.-H. Tsai, J.-R. Wu, S.-J. Chen, J.-H. Lii, H.-M. Lee, Organometallics, 29 (2010) 6473-6481.
[22] S.-Y. Chang, J.-L. Chen, Y. Chi, Y.-M. Cheng, G.-H. Lee, C.-M. Jiang, P.-T. Chou, Inorg. Chem., 46 (2007) 11202-11212.
[23] S.-Y. Chang, J. Kavitha, J.-Y. Hung, Y. Chi, Y.-M. Cheng, E.Y. Li, P.-T. Chou, G.-H. Lee, A.J. Carty, Inorg. Chem., 46 (2007) 7064-7074.
[24] C. Cuerva, J.A. Campo, P. Ovejero, M.R. Torres, M. Cano, Dalton Trans., 43 (2014) 8849-8860.
[25] C. Cuerva, J.A. Campo, P. Ovejero, M.R. Torres, E. Oliveira, S.M. Santos, C. Lodeiro, M. Cano, J. Mater. Chem. C, 2 (2014) 9167-9181.
[26] L. Holland, W.-Z. Shen, P. von Grebe, P.J. Sanz Miguel, F. Pichierri, A. Springer, C.A. Schalley, B. Lippert, Dalton Trans., 40 (2011) 5159-5161.
[27] H.-Y. Hsieh, C.-H. Lin, G.-M. Tu, Y. Chi, G.-H. Lee, Inorg. Chim. Acta, 362 (2009) 4734-4739.
[28] A. Satake, H. Koshino, T. Nakata, J. Organomet. Chem., 595 (2000) 208-214.
[29] M.D. Ward, J.S. Fleming, E. Psillakis, J.C. Jeffery, J.A. McCleverty, Acta Crystallogr., Sect. C: Cryst. Struct. Commun., C54 (1998) 609-612.
[30] Z. Qin, H.A. Jenkins, S.J. Coles, K.W. Muir, R.J. Puddephatt, Can. J. Chem., 77 (1999) 155-157.
[31] Z. Qin, M.C. Jennings, R.J. Puddephatt, K.W. Muir, Inorg. Chem., 41 (2002) 5174-5186.
[32] Z.Q. Qin, M.C. Jennings, R.J. Puddephatt, K.W. Muir, CrystEngComm, (2000) 73-76.
[33] A. Kovacs, Z. Varga, Coord. Chem. Rev., 250 (2006) 710-727.
[34] D.P. Malenov, D.B. Ninkovic, D.N. Sredojevic, S.D. Zaric, ChemPhysChem, 15 (2014) 2458-2461.
[35] D.N. Sredojevic, D.B. Ninkovic, G.V. Janjic, J. Zhou, M.B. Hall, S.D. Zaric, ChemPhysChem, 14 (2013) 1797-1800.
[36] K. Molcanov, M. Juric, B. Kojic-Prodic, Dalton Trans., 42 (2013) 15756-15765.
[37] D.N. Sredojevic, D.Z. Vojislavljevic, Z.D. Tomic, S.D. Zaric, Acta Crystallogr., Sect. B: Struct. Sci., 68 (2012) 261-265.
[38] D.N. Sredojevic, Z.D. Tomic, S.D. Zaric, Cryst. Growth Des., 10 (2010) 3901-3908.
[39] D. Sredojevic, G.A. Bogdanovic, Z.D. Tomic, S.D. Zaric, CrystEngComm, 9 (2007) 793-798.
[40] K. Molcanov, M. Curic, D. Babic, B. Kojic-Prodic, J. Organomet. Chem., 692 (2007) 3874-3881.
[41] Y. Sako, S. Ichikawa, A. Osada, A. Matsuda, Bioorg. Med. Chem., 18 (2010) 7878-7889.
[42] P. Kanoo, R. Matsuda, H. Sato, L. Li, H.J. Jeon, S. Kitagawa, Inorg. Chem., 52 (2013) 10735-10737.
[43] A.J. Amoroso, A.M.C. Thompson, J.C. Jeffery, P.L. Jones, J.A. McCleverty, M.D. Ward, J. Chem. Soc., Chem. Commun., (1994) 2751-2752.
[44] T. Mosmann, J. Immunol. Methods, 65 (1983) 55-63.
[45] T. Mosmann, J Immunol Methods, 65 (1983) 55-63.
[46] CrysAlisPRO, in, Oxford Diffraction / Agilent Technologies UK Ltd, Yarton, England, 2012.
[47] A. Altomare, M.C. Burla, M. Camalli, G.L. Cascarano, C. Giacovazzo, A. Guagliardi, A.G.G. Moliterni, G. Polidori, R. Spagna, J. Appl. Crystallogr., 32 (1999) 115-119.

[48] G.M. Sheldrick, Acta Crystallogr., Sect. A: Found. Crystallogr., 64 (2008) 112-122.
[49] L.J. Farrugia, J. Appl. Crystallogr., 32 (1999) 837-838.
[50] M.J. Frisch, et. al., in, Gaussian Inc., Wallingford CT., 2009.
[51] D.A. McMorran, P.J. Steel, Inorg. Chem. Commun., 6 (2003) 43-47.
[52] D.A. McMorran, P.J. Steel, Chem. Commun. (Cambridge, U. K.), (2002) 2120-2121.
[53] C. Janiak, Dalton, (2000) 3885-3896.
[54] L. Yang, D.R. Powell, R.P. Houser, Dalton Trans., (2007) 955-964.
[55] G.V. Janjic, S.D. Zaric, Noncovalent interactions of π-systems in crystal structures of transition-metal complexes, in: The Importance of Pi-Interactions in Crystal Engineering, John Wiley & Sons Ltd., 2012, pp. 243-274.
[56] R. Horvath, M.G. Fraser, S.A. Cameron, A.G. Blackman, P. Wagner, D.L. Officer, K.C. Gordon, Inorg. Chem., 52 (2013) 1304-1317.
[57] M.A. Spackman, D. Jayatilaka, CrystEngComm, 11 (2009) 19-32.
[58] J.J. McKinnon, A.S. Mitchell, M.A. Spackman, Chem. - Eur. J., 4 (1998) 2136-2141.
[59] S.K.G. Wolff, D. J.; McKinnon, J. J.; Turner, M. J.; Jayatilaka, D.; Spackman, M. A., (2012) University of Western Australia.
[60] C.F. Macrae, P.R. Edgington, P. McCabe, E. Pidcock, G.P. Shields, R. Taylor, M. Towler, J. van de Streek, J. Appl. Crystallogr., 39 (2006) 453-457.
[61] N.J. Wheate, S. Walker, G.E. Craig, R. Oun, Dalton Trans., 39 (2010) 8113-8127.
[62] A.R. Kapdi, I.J.S. Fairlamb, Chem. Soc. Rev., 43 (2014) 4751-4777.
[63] C. Icsel, V.T. Yilmaz, F. Ari, E. Ulukaya, W.T.A. Harrison, Eur. J. Med. Chem., 60 (2013) 386-394.
[64] R.M. Medina, J. Rodriguez, A.G. Quiroga, F.J. Ramos-Lima, V. Moneo, A. Carnero, C. Navarro-Ranninger, M.J. Macazaga, Chem. Biodiversity, 5 (2008) 2090-2100.
[65] F.J. Ramos-Lima, A.G. Quiroga, J.M. Perez, C. Navarro-Ranninger, Polyhedron, 22 (2003) 3379-3381.
[66] Y.-g. Sun, D. Sun, W. Yu, M.-c. Zhu, F. Ding, Y.-n. Liu, E.-j. Gao, S.-j. Wang, G. Xiong, I. Dragutan, V. Dragutan, Dalton Trans., 42 (2013) 3957-3967.
[67] Y.-g. Sun, Y. Guo, D. Sun, M.-c. Zhu, F. Ding, Y.-n. Liu, E.-j. Gao, S.-j. Wang, G. Xiong, I. Dragutan, V. Dragutan, Eur. J. Inorg. Chem., 2014 (2014) 5741-5751.
[68] B.D. Lehmann, J.A. Bauer, X. Chen, M.E. Sanders, A.B. Chakravarthy, Y. Shyr, J.A. Pietenpol, J. Clin. Invest., 121 (2011) 2750-2767.
[69] W.K.C. Lo, G.S. Huff, D. Preston, D.A. McMorran, G.I. Giles, K.C. Gordon, J.D. Crowley, Inorganic Chemistry, 54 (2015) 6671-6673.
[70] S.M. McNeill, D. Preston, J.E.M. Lewis, A. Robert, K. Knerr-Rupp, D.O. Graham, J.R. Wright, G.I. Giles, J.D. Crowley, Dalton Trans., 44 (2015) 11129-11136.

# Palladium(II) and Platinum(II) Complexes of ((2-pyridyl)pyrazol-1-ylmethyl)benzoic Acids: Synthesis, Solid State Characterisation and Biological Cytotoxicity.

Aidan P McKay[1], Warrick K C Lo[1], Dan Preston[1], Gregory I Giles[2], James D Crowley[1], Jonathan E Barnsley[1], Keith C Gordon[1] and David A McMorran[1]*

HIGHLIGHTS

1. Pd(II) and Pt(II) complexes containing ligands with both metal binding sites and distal hydrogen-bonding sites are reported and structurally characterised.
2. Assembly of the complexes is found to be mediated by both hydrogen bonding interactions and π-stacking interactions, many of which involve the chelate rings.
3. Hirshfeld surface analysis provides quantitative insight into how complex assembly varies with ligand and metal ion.

**Graphical Abstract**

[$PdCl_2$(**L**)] and [$PtCl_2$(**L**)] complexes of ((2-pyridyl)pyrazol-1-ylmethyl)benzoic acids have been prepared and characterised. In the solid state molecules assemble *via* π(chelate)-stacking and a variety of hydrogen bonding motifs, the natures of which was also explored using Hirshfeld surface analysis and DFT calculations. Cytotoxicity studies on the [$PtCl_2$(**L**)] complexes are also reported.